Conformational Properties of a Back-Folding Wormlike Chain Confined in a Cylindrical Tube

Jeff Z. Y. Chen*
Department of Physics and Astronomy, University of Waterloo, Waterloo, Ontario N2L 3G1, Canada
(Received 8 March 2017; published 16 June 2017)

When a semiflexible chain is confined in a narrow cylindrical tube, the formation of a polymer hairpin is a geometrical conformation that accompanies an exponentially large local free energy and, hence, is a relatively rare event. Numerical solutions of the hairpin distribution functions for persistence-length-to-tube-radius ratios over a wide range are obtained in high precision, by using the Green's function approach for the wormlike-chain model. The crossover region between the narrow and moderately narrow tubes is critically investigated in terms of the hairpin free energy, global persistence length, mean hairpin-tip distance from the tube axis, and hairpin-plane orientational properties. Accurate representations of the solutions by simple interpolation formulae are suggested.

DOI: 10.1103/PhysRevLett.118.247802

Introduction.—The coarse-grained wormlike chain serves as a foundation in statistical physics to support our understanding of semiflexible polymer chains. Originally presented in a discrete form [1], the model is more conveniently described in a continuum form by treating the polymer as a string of length L [2], which nowadays can be used to exploit the similarity between the mathematical structures of the polymer theory and the quantum field theory [3,4]. The persistence length P is a characteristic length scale in the model that describes the orientation-orientation correlation length between polymer segments along the chain, in free space [2,5].

When the chain is confined in a narrow tube of diameter D, the orientation-orientation correlation is drastically altered, and two length scales emerge: the deflection length λ, which describes the average length of polymer segments that are free from the wall interaction [6], and the global persistence length g that as an effective step length renormalizes the system into an one-dimensional random walk on a large scale [7] (see Fig. 1). Experimental [8–14] and theoretical [7,15–28] understandings of a DNA molecule in various forms of confinement, for example, heavily depend on these fundamental concepts. While the dependence of λ on P and D is relatively well understood, the precise theoretical understanding of the dependence of g on these parameters remains unclear, despite its importance. This Letter aims at providing a thorough analysis of the problem and reconciling the current mismatch between the Monte Carlo data [27] and the *only* theoretical result in the literature [7].

In the wormlike-chain (WLC) model, the quadratic curvature of a polymer segment is penalized by a bending-energy parameter directly proportional to P. As such, the model gives rise to the leading contribution to a hairpin free energy (reduced by $\beta^{-1} = k_B T$, where k_B is the Boltzmann constant and T the temperature), $E_m P/r$, where $2r$ is the distance between the two parallel stick segments and E_m is a numerical coefficient. On the basis of this model, Odijk deduced an optimal hairpin shape, taking the theoretical approach that ignores all hairpin shape fluctuations, in terms of the mechanical-limit approximation [7], at the same level as the classical-trajectory theory [29]. In addition, he effectively took the translational entropy into account, considering the degrees of freedom associated with moving a hairpin on a tube cross section as the partial contribution to the hairpin free energy F_0, and arrived at

$$\beta F_0^{\mathrm{Od}}(\tilde{D}) = \frac{E_m}{\tilde{r}} - \frac{3}{2}\ln\left[\frac{(\tilde{D}/2 - \tilde{r})}{\tilde{D}/2}\right] - \ln\left(\frac{\sqrt{8.2}}{3\pi}\right), \quad (1)$$

where

$$\tilde{r} = [(E_m^2 + 3E_m\tilde{D})^{1/2} - E_m]/3. \quad (2)$$

In this Letter, all tilded symbols are scaled by P such that $\tilde{D} = D/P$ and $\tilde{r} = r/P$. Following an argument for one-dimensional dilute defects, he further deduced the global persistence length

$$\tilde{g}^{\mathrm{Od}}(\tilde{D}) = \alpha\tilde{r}\exp(\beta F^{\mathrm{Od}}), \quad (3)$$

where α is the ratio between l, half of the contour length of the hairpin curve, and r. All these were proposed for small $\tilde{D}$, forming our previous theoretical understanding [7].

Here three basic questions are examined, based on the numerical solutions to the exact, Green's function formalism of the WLC [3] over the entire $\tilde{D}$ range, after a careful treatment of the boundary condition to address the hard-wall confinement [30]. First, how accurate are the Odijk approximants, (1) and (2), to represent the WLC solution in the small-$\tilde{D}$ regime? When the expressions were compared with recent Monte Carlo data calculated for g in the moderately narrow channels, Muralidhar and Dorfman discovered that $\tilde{g}^{\mathrm{Od}}$ is off by *2 orders of magnitude* in

the $\tilde{D}$ range (1,2); hence, they suggested that a constant shift in βF^{Od} is needed to remedy the difference for this range, locally [27]. The exact solution to the problem for g presented here for cylindrical-tube confinement agrees with Muralidhar and Dorfman's Monte Carlo data in order of magnitude within the same $\tilde{D}$ range. A lesser but unignorable problem is that Odijk made an algebraic mistake in calculating E_m and α [7]; a new derivation presented in Supplemental Material [31], closely following his treatment, yields the differences

$$E_m(\mathrm{Odijk}) = 1.5071\ldots, \quad E_m(\mathrm{corrected}) = 1.43557\ldots \tag{4}$$

and

$$\alpha(\mathrm{Odijk}) = 3.3082\ldots, \quad \alpha(\mathrm{corrected}) = 4.4149\ldots. \tag{5}$$

These corrections do affect the asymptotically small-$\tilde{D}$ regime where the leading term in (1) survives but do not constitute a significant correction to the numerical values of (3) in the moderate-$\tilde{D}$ range (1,2).

We hence face the second question: Can one develop a simple representation of the (exact) numerical solutions of both βF and $\tilde{g}$ for the entire $\tilde{D}$ range, *globally*? As it turns out, we well understand the $\tilde{D} \gg 1$ asymptotic limit: $\beta F = \ln 4$ using a simple argument and $\tilde{g} = 1$ by definition. As demonstrated below, both

$$\beta F_0(\tilde{D}) = \frac{2E_m}{\tilde{D}} - \frac{3}{2}\ln\left[\frac{A_2\tilde{D} + A_0\tilde{D}^2}{1 + A_1\tilde{D} + A_0\tilde{D}^2}\right] + \ln 4 \tag{6}$$

and

$$\ln\tilde{g}(\tilde{D}) = \frac{2E_m}{\tilde{D}} - \frac{1}{2}\ln\left[\frac{B_2\tilde{D} + B_0\tilde{D}^2}{1 + B_1\tilde{D} + B_0\tilde{D}^2}\right] \tag{7}$$

are viable and accurate representations of the exact solutions, where the numerical values of the constants are $A_0 = 1.0410$, $A_1 = -0.6046$, $A_2 = 1.2150$, $B_0 = 1.2907$, $B_1 = -1.4449$, and $B_2 = 5.9560$. The coefficients of the logarithmic terms in these expressions, $-3/2$ and $-1/2$, are maintained here according to Eqs. (1)–(3).

Finally, are there any other statistical properties that we can use for a better understanding of hairpin conformations? Discussed below are the distribution function of the distance between the tube axis to the hairpin tip (i.e., the point on the hairpin where the polymer makes a U turn) and the orientational distribution of the hairpin planes. These enable a more clear-cut physical picture beyond the entropy-depletion idea.

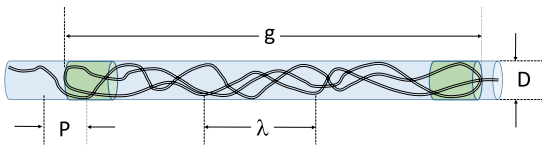

FIG. 1. Sectional illustration of a tube of diameter D, which contains two hairpins formed by the confined polymer segment. The polymer makes a one-dimensional random walk along the tube axis with an effective, long step length $2g$.

Hairpin free energy.—A number of physical properties of the WLC can be accessed through the reduced Green's function $q(\mathbf{r}, \mathbf{u})$, also named the "propagator"; it describes the probability of finding one terminal end of a polymer in the vicinity of a spatial point described by the positional vector $\mathbf{r}$ and with a tangent vector pointing in a direction described by a unit vector $\mathbf{u}$. The properties of the other end do not matter provided that an extremely long polymer is concerned ($L \gg g$). Within this limit, the ground-state-dominance approximation [32] is exact, such that $q(\mathbf{r}, \mathbf{u})$ is the ground-state eigenfunction that satisfies [3,30]

$$-\beta\mu q(\mathbf{r}, \mathbf{u}) = [-2P\mathbf{u}\cdot\boldsymbol{\nabla}_{\mathbf{r}}|_{\mathbf{u}} + \nabla^2_{\mathbf{u}} - 2PU_{\mathrm{ext}}(\mathbf{r}, \mathbf{u})]q(\mathbf{r}, \mathbf{u}), \tag{8}$$

where μ, the ground-state eigenvalue, is the confinement free energy per "Kuhn" segment of length $2P$. Much previous attention was placed on obtaining $\beta\mu \propto \tilde{D}^{-2/3}$ in the Odijk regime and understanding its relationship with λ [6,20,33–41], by various theoretical and simulation methods including directly solving the above equation [41]. The external potential experienced by a unit contour length, U_{ext}, is always zero but is introduced here to calculate χ below.

Cylindrical coordinates are used here, in which the tube axis is defined as the z axis with a unit vector $\hat{\mathbf{z}}$. The distribution function has a rotational symmetry about $\hat{\mathbf{z}}$ and a translational symmetry along the $\hat{\mathbf{z}}$; hence, one needs only to take the distance to the axis, ρ, as the spatial dependence, with the corresponding unit vector $\hat{\boldsymbol{\rho}}$ directed away from the z axis [42]. An additional spherical coordinate system containing polar and azimuth angles θ, φ is established for $\mathbf{u}$ such that $\mathbf{u}\cdot\hat{\mathbf{z}} = \cos\theta$ and $\mathbf{u}\cdot\hat{\boldsymbol{\rho}} = \sin\theta\cos\varphi$. Special attention must be paid to properly expressing the derivative term $\mathbf{u}\cdot\boldsymbol{\nabla}_{\mathbf{r}}|_{\mathbf{u}}$ in cylindrical coordinates [30,43]. Then, the five-variable function $q(\mathbf{r}, \mathbf{u})$ is represented by the three-variable function $q(\rho, \theta, \varphi)$. The unnormalized segmental density distribution is found from $f(\mathbf{r}, \mathbf{u}) = q(\mathbf{r}, \mathbf{u})q(\mathbf{r}, -\mathbf{u})$, or $f(\rho,\theta,\varphi) = q(\rho,\theta,\varphi)q(\rho,\pi-\theta,\pi+\varphi)$. The probability function of finding a hairpin tip is given by

$$f_0(\rho, \varphi) = f(\rho, \pi/2, \varphi)/2C, \tag{9}$$

where $C = \int_0^{\pi} d\theta \sin\theta \int_0^{2\pi} d\varphi \int_0^{D/2} d\rho\rho f(\rho, \theta, \varphi)$ is the normalization constant. The $1/2$ factor takes into account the fact that, out of all configurations that are described by $f(\rho, \pi/2, \varphi)$, only $1/2$ are hairpin tips, and the other $1/2$ are inflection points. The hairpin free energy can then be obtained from $\beta F_0 = -\ln[\int d\varphi \int d\rho\rho f_0]$.

The squares in Fig. 2(a) represent the numerical solutions. The data in the limit $\tilde{D} \ll 1$ converge to the first term in

Eq. (6), $2E_m/\tilde{D}$, which is represented by the black solid line; this reflects the physical picture that the dominating contribution to βF_0 is from the bending energy. In the large-$\tilde{D}$ regime, the polymer can be regarded as a flexible chain, and all $\mathbf{u}$ dependence disappears, which yields $\beta F_0 = \ln 4$ according to the above definition. The interpolation curve, given in Eq. (6) and plotted as the red solid curve in Fig. 2, asymptotically approaches this constant.

Global persistence length.—Formally, the mean-square end-to-end distance along the tube axis can be calculated by introducing a virtual external potential

$$U_{\text{ext}} = -\frac{\epsilon}{P}\hat{\mathbf{z}}\cdot\mathbf{u} \tag{10}$$

into (8), as suggested by Khokhlov and Semenov for the liquid-crystal theory of wormlike polymers [44]. One can then obtain

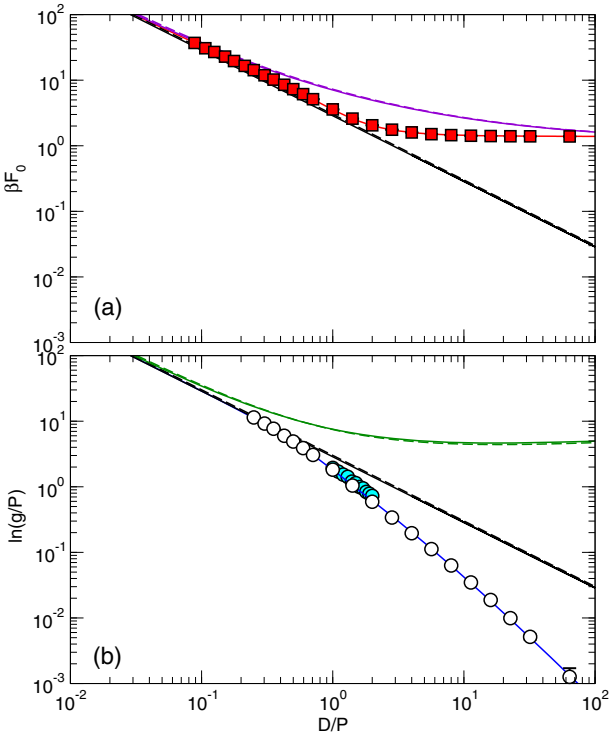

FIG. 2. Hairpin free energy βF_0 and global persistence length g as functions of the reduced tube diameter D/P. Common to the two plots are dashed and solid black lines representing the asymptotic behavior $2E_m/\tilde{D}$ with Odijk's and the corrected values in (4), respectively. In plot (a), squares represent the exact solutions for βF_0 obtained in this work with the underlying red curve plotted according to (6). The purple curves are (1) with Odijk's (dashed) and corrected (solid) E_m values stated in (4). In plot (b), open circles represent the exact solutions for $\ln g/P$ obtained in this work with the underlying curve plotted according to (7). The green curves are (3), which are produced with the additional α values listed in (5): dashed for Odijk's and solid for the corrected. The filled circles are the Monte Carlo data for g/P provided by authors of Ref. [27].

$$\langle R_z^2\rangle = LP\chi, \tag{11}$$

where χ is the susceptibility $\partial\langle\hat{\mathbf{z}}\cdot\mathbf{u}\rangle/\partial\epsilon$ evaluated at $\epsilon = 0$. The calculation can be further simplified by a first-order perturbation theory in ϵ, which splits (8) into two partial differential equations [45]. The definition

$$\tilde{g} = 3\chi/2(1+2m) \tag{12}$$

is adopted here for a $L \gg g$ chain, where $m = [3\langle(\hat{\mathbf{z}}\cdot\mathbf{u})^2\rangle - 1]/2$ is the orientational order parameter [28,46]. All technical details of the numerical treatment can be found in Supplemental Material [31].

The numerical solution for $\ln\tilde{g}$ obtained this way is displayed by unfilled circles in Fig. 2(b) in a logarithmic plot. Note that the vertical scale is actually $\log(\ln\tilde{g})$. The data can be well captured by the empirical equation, (7), over the entire $\tilde{D}$ range, which is plotted as the blue solid curve. In the small-$\tilde{D}$ limit, $\ln\tilde{g}$ approaches $2E_m/\tilde{D}$, and in the large-$\tilde{D}$ limit, $\ln\tilde{g}$ approaches 0 as g becomes P. For comparison, the Odijk approximant (3) for $\tilde{g}$, plotted as the green curves, with his and the corrected constants in (4) and (5), are indeed off by orders of magnitude in the $\tilde{D}$ range (1,2), as noted in Ref. [27].

Hairpin conformations.—The solution of the Green's function provides further insights into how $\tilde{D}$ controls different types of hairpin conformations. For this purpose, two distribution functions are examined together. The normalized distributions of hairpin tips,

$$H\left(\frac{2\rho}{D}\right) = \frac{D^2}{4}\int d\varphi f_0\left(\frac{2\rho}{D},\varphi\right)\Big/\int_0^{D/2} d\rho\rho\int d\varphi f_0\left(\frac{2\rho}{D},\varphi\right), \tag{13}$$

are illustrated in Fig. 3(a) and 3(b), based on which the mean distances of the hairpin tips to the axis, $\langle\rho\rangle$, are determined and displayed in Fig. 3(c) for various $\tilde{D}$. To measure the mean orientations of the tangent vectors at hairpin tips, $\mathbf{u}$, as a function of the tip-to-axis distance,

$$\sigma\left(\frac{2\rho}{D}\right) = \int d\varphi(\cos 2\varphi) f_0\left(\frac{2\rho}{D},\varphi\right)\Big/\int d\varphi f_0\left(\frac{2\rho}{D},\varphi\right) \tag{14}$$

is considered. In the ideal case of isotropic projections of $\mathbf{u}$ on a tube cross section, $\sigma = 0$; in the other ideal case of a strong directional distribution along $\hat{\mathbf{z}}\times\hat{\rho}$, $\sigma = -1$ (see Fig. 3, inset). Figure 4 illustrates the profiles $\sigma(2\rho/D)$ for various $\tilde{D}$. Two obvious features can be seen: at $\rho = D/2$, because of the wall presence $\sigma = -1$ for *all* $\tilde{D}$, and at $\rho = 0$, because of the symmetry about the tube axis $\sigma = 0$ for *all* $\tilde{D}$, all consistent with the physical intuition. What comes as a surprise is the peak of $\langle\rho\rangle$ in Fig. 3(c) at $\tilde{D}\approx 2$. The hairpin conformations are discussed from large to small $\tilde{D}$ below.

The density profile for the asymptotic limit $\tilde{D} \gg 1$ can be analytically determined, as the orientation dependence disappears; the hairpin planes at the tips display an isotropic distribution without a bending energy penalty [illustrated by blue and red arrows in Fig. 4(b)]; hence, $\sigma = 0$ in most ρ regions. The WLC model then reduces to a two-dimensional Gaussian-chain model on the tube cross-section plane, on which the normalized hairpin-tip distribution can be analytically derived [47]:

$$H(2\rho/D) = 2J_0^2(2k\rho/D)/J_1^2(k), \tag{15}$$

where $J_n(x)$ is the Bessel function of order n and $k = 2.40483\ldots$ is the first root of $J_0(k) = 0$. One can then analytically determine $2\langle\rho\rangle/D = 0.4240\ldots$, which is exactly the asymptotic limit of the numerical solutions in Fig. 3(c) for large $\tilde{D}$.

In the first crossover region $(2, \infty)$, as $\tilde{D}$ is lowered, more directionally ordered hairpin tips start to show up near the inner surface; this is particularly so in a system with $\tilde{D} \gtrsim 2$, reflected by the increasing range of ρ near the tube surface with negative σ, shown in Fig. 4(a). As the bending energy prefers a bigger hairpin loop, the geometric requirement pushes the hairpin tips away from the tube axis and forces the hairpin plane to bend [Fig. 4(c)]. The distribution $H(2\rho/D)$ in Fig. 3(b) is hence broadened from the profile at $\tilde{D} \gg 1$ (dashed curve) to accommodate this pushing away.

Within the second crossover region, $\tilde{D} = (10^{-1}, 2)$, the increasing rigidity prefers the entire hairpin to be more coplanar while maximizing the hairpin size. This tendency now brings more hairpin tips to the tube axis. Those near the tube surface are even more ordered, $\sigma \sim -1$ (Fig. 4), but become rarer events. The narrowing of the distribution function $H(2\rho/D)$ [Fig. 3(a)] is the direct cause of this requirement. This is a crossover range that are currently accessible through Monte Carlo simulations [26–28] and is probably most relevant in a real experimental setting. The logarithmic correction term in (1) was an attempt to address this region, in terms of the depletion entropy associated with the translational degree of freedom of the hairpin tips, which was estimated by the assumption that the hairpin planes are fixed in parallel to $\hat{\mathbf{z}}$ [7]. The assumption, however, underestimates the entropic contributions; for systems where $\tilde{D} \sim 1$, hairpin planes can undergo further wobbling motion against the hairpin tips, shown schematically by the red arrows in Fig. 4(c), in addition to the translational degrees of freedom shown by yellow and blue arrows. Hence, quantities such as βF_0 and $\ln \tilde{g}$ significantly deviate from (1) and (3) in the second crossover region.

Finally, in the asymptotic limit $\tilde{D} \ll 1$, which exists in the range $\tilde{D} < 10^{-1}$ according to our data, a hairpin loses most shape fluctuations, and the distance between the hairpin tip to the axis, ρ, is vanishingly small as the hairpin configurations approach the classical-trajectory shape. One expects that $2\langle\rho\rangle/D$ follows the power-law scaling

$$2\langle\rho\rangle/D = \gamma\tilde{D}^{1/2} (\tilde{D} \ll 1) \tag{16}$$

as $H(x)$ asymptotically approaches a normal distribution of ρ/D with a variation width $\langle\rho\rangle/D$. The coefficient can be estimated from the numerical solution presented in Fig. 3(c)

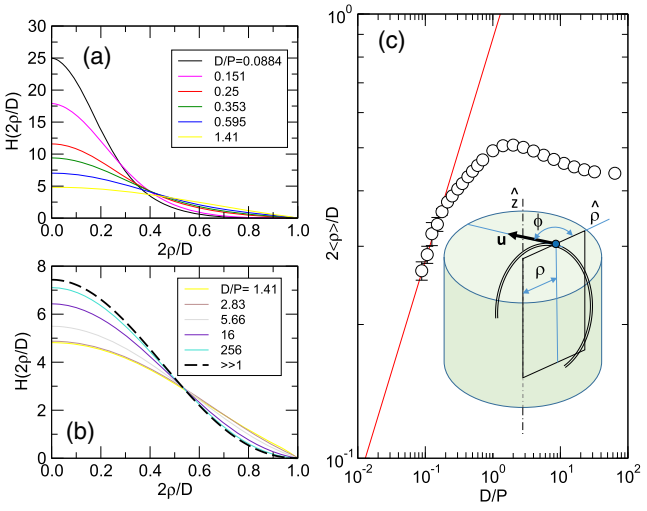

FIG. 3. (a),(b) Hairpin-tip distributions as functions of $2\rho/D$ for various $\tilde{D}$ and (c) mean hairpin tip to axis distance $\langle\rho\rangle$ as a function of $\tilde{D}$. The inset in (c) shows a hairpin tip specified by a blue circle located at ρ with a unit vector $\mathbf{u}$ making an angle φ with $\hat{\rho}$.

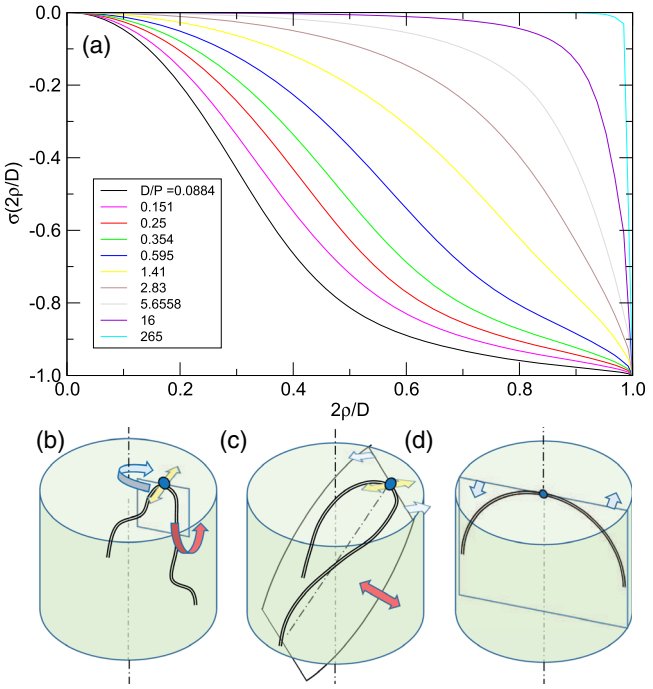

FIG. 4. (a) Parameter measuring the directional ordering of the tangent directions of hairpin tips, σ, as a function of the hairpin distance from the tube axis, as well as (b)–(d) examples of hairpin configurations where the hairpin tips are labeled by blue circles. Plots (b)–(d) correspond to the parameter regimes $\tilde{D} \gg 1$, ~ 1, and $\ll 1$, respectively.

by circles, $\gamma = 0.88 \pm 0.04$. The behaviors of both βF_0 and $\ln \tilde{g}$ are dominated by the leading bending energy term.

Summary.—In this study, the conformational properties of WLC hairpins in a confining cylindrical tube are analyzed through the numerical solution for the probability function. In the first part, the discussion is geared towards clarifying the confusion caused by the previous theoretical results for the hairpin free energy and global persistence length; that the Odijk approximants require modification in the crossover region is demonstrated, and new accurate representations are proposed for a wide range of D/P. In the second part, the free energies associated with bending hairpin planes and wobbling degrees of freedom are argued to be important, changing the physical picture of hairpin conformational properties based on the translational "depletion" entropy assumption. Two crossover regions are identified, each having different hairpin-plane properties. These predictions should be directly verifiable by using Monte Carlo methods. The current work is for a phantom WLC. It paves the way for the next step of including the excluded volume interactions in the theory, which is an active research area where Monte Carlo studies have just emerged [26–28] and previous scaling arguments exist [16,25].

Financial support from the Natural Sciences and Engineering Council of Canada is gratefully acknowledged. This work was made possible by the facilities of the Shared Hierarchical Academic Research Computing Network and Compute Canada. The author thanks Drs. Muralidhar and Dorfman who provided the original Monte Carlo data plotted in Fig. 2(b).

*jeffchen@uwaterloo.ca

[1] O. Kratky and G. Porod, Recl. des Trav. Chim. des Pays-Bas **68**, 1106 (1949).
[2] N. Saitô, K. Takahashi, and Y. Yunoki, J. Phys. Soc. Jpn. **22**, 219 (1967).
[3] K. F. Freed, Adv. Chem. Phys. **22**, 1 (1972).
[4] M. Doi and S. F. Edwards, *The Theory of Polymer Dynamics* (Oxford University, New York, 1988).
[5] P. G. de Gennes, *Scaling Concepts in Polymer Physics* (Cornell University, Ithaca, 1979).
[6] T. Odijk, Macromolecules **16**, 1340 (1983).
[7] T. Odijk, J. Chem. Phys. **125**, 204904 (2006).
[8] W. Reisner, K. J. Morton, R. Riehn, Y. M. Wang, Z. Yu, M. Rosen, J. C. Sturm, S. Y. Chou, E. Frey, and R. H. Austin, Phys. Rev. Lett. **94**, 196101 (2005).
[9] J. T. D. Bonis-O'Donnell, W. Reisner, and D. Stein, New J. Phys. **11**, 075032 (2009).
[10] W. Reisner, J. N. Pedersen, and R. H. Austin, Rep. Prog. Phys. **75**, 106601 (2012).
[11] D. Gupta, J. Sheats, A. Muralidhar, J. J. Miller, D. E. Huang, S. Mahshid, K. D. Dorfman, and W. Reisner, J. Chem. Phys. **140**, 214901 (2014).
[12] A. R. Klotz, L. Duong, M. Mamaev, H. W. de Haan, J. Z. Y. Chen, and W. W. Reisner, Macromolecules **48**, 5028 (2015).
[13] D. Gupta, J. J. Miller, A. Muralidhar, S. Mahshid, W. Reisner, and K. D. Dorfman, ACS Macro Lett. **4**, 759 (2015).
[14] J.-W. Yeh and K. Szeto, ACS Macro Lett. **5**, 1114 (2016).
[15] Y.-L. Chen, H. Ma, M. D. Graham, and J. J. de Pablo, Macromolecules **40**, 5978 (2007).
[16] T. Odijk, Phys. Rev. E **77**, 060901 (2008).
[17] P.-K. Lin, K.-H. Lin, C.-C. Fu, K.-C. Lee, P.-K. Wei, W.-W. Pai, P.-H. Tsao, Y.-L. Chen, and W. S. Fann, Macromolecules **42**, 1770 (2009).
[18] Y. Wang, D. R. Tree, and K. D. Dorfman, Macromolecules **44**, 6594 (2011).
[19] P.-K. Lin, C.-C. Hsieh, Y.-L. Chen, and C.-F. Chou, Macromolecules **45**, 2920 (2012).
[20] M. R. Smyda and S. C. Harvey, J. Phys. Chem. B **116**, 10928 (2012).
[21] R. Chang and K. Jo, J. Chem. Phys. **136**, 095101 (2012).
[22] Z. Benkova and P. Cifra, Macromolecules **45**, 2597 (2012).
[23] D. R. Tree, Y. Wang, and K. D. Dorfman, Phys. Rev. Lett. **110**, 208103 (2013).
[24] L. Dai, D. R. Tree, J. R. C. van der Maarel, K. D. Dorfman, and P. S. Doyle, Phys. Rev. Lett. **110**, 168105 (2013).
[25] L. Dai, J. van der Maarel, and P. S. Doyle, Macromolecules **47**, 2445 (2014).
[26] A. Muralidhar, D. R. Tree, and K. D. Dorfman, Macromolecules **47**, 8446 (2014).
[27] A. Muralidhar and K. D. Dorfman, Macromolecules **49**, 1120 (2016).
[28] A. Muralidhar, M. J. Quevillon, and K. D. Dorfman, Polymers **8**, 79 (2016).
[29] S. T. Milner, T. A. Witten, and M. E. Cates, Macromolecules **21**, 2610 (1988).
[30] J. Z. Y. Chen, Prog. Polym. Sci. **54–55**, 3 (2016).
[31] See Supplemental Material at http://link.aps.org/supplemental/10.1103/PhysRevLett.118.247802 for mathematical details.
[32] A. Y. Grosberg and A. R. Khokhlov, *Statistical Physics of Macromolecules* (AIP, New York, 1994).
[33] T. Odijk, Macromolecules **19**, 2313 (1986).
[34] T. W. Burkhardt, J. Phys. A **28**, L629 (1995).
[35] M. Dijkstra, D. Frenkel, and H. N. Lekkerkerker, Physica A (Amsterdam) **193**, 374 (1993).
[36] T. W. Burkhardt, J. Phys. A **30**, L167 (1997).
[37] D. J. Bicout and T. W. Burkhardt, J. Phys. A **34**, 5745 (2001).
[38] Y. Yang, T. W. Burkhardt, and G. Gompper, Phys. Rev. E **76**, 011804 (2007).
[39] T. W. Burkhardt, Y. Yang, and G. Gompper, Phys. Rev. E **82**, 041801 (2010).
[40] H.-P. Hsu and K. Binder, Soft Matter **9**, 10512 (2013).
[41] J. Z. Y. Chen, Macromolecules **46**, 9837 (2013).
[42] G. B. Arfken, H.-J. Weber, and L. Ruby, *Mathematical Methods for Physicists* (Academic, New York, 1985).
[43] Q. Liang, J. Li, P. Zhang, and J. Z. Y. Chen, J. Chem. Phys. **138**, 244910 (2013).
[44] A. R. Khokhlov and A. N. Semenov, J. Phys. A **15**, 1361 (1982).
[45] G. J. Vroege and T. Odijk, Macromolecules **21**, 2848 (1988).
[46] A. Tkachenko and Y. Rabin, Macromolecules **28**, 8646 (1995).
[47] J. Gao, P. Tang, Y. Yang, and J. Z. Y. Chen, Soft Matter **10**, 4674 (2014).